Fourier Transform Infrared spectroscopy discloses different types of cell death in flow cytometrically sorted cells

K. le Roux,[a] L.C. Prinsloo[b] and D. Meyer[a,c*]

[a] Department of Biochemistry, University of Pretoria, Hatfield, Gauteng, 0002, South Africa.

[b] Department of Physics, University of Pretoria, Hatfield, Gauteng, 0002, South Africa.

[c] Department of Biochemistry, University of Johannesburg, Auckland Park, Gauteng, 2006, South Africa.

Abstract

Fourier Transform Infrared (FTIR) spectroscopy is a label free methodology showing promise in characterizing different types of cell death. Cervical adenocarcinoma (HeLa) and African monkey kidney (Vero) cells were treated with a necrosis inducer (methanol), novel apoptotic inducers (diphenylphosphino gold (I) complexes) and positive control, auranofin. Following treatment, cells stained with annexin-V and propidium iodide were sorted using a Fluorescence Activated Cell Sorter (FACS Aria) to obtain populations consisting of either viable, necrotic or apoptotic cells. Transmission Electron Microscopy confirmed successful sorting of all three populations. Four bands were identified which could discriminate between viable and necrotic cells namely 989 cm^{-1}, 2852 cm^{-1}, 2875 cm^{-1} and 2923 cm^{-1}. In HeLa cells viable and induced apoptosis could be distinguished by 1294 cm^{-1}, while four bands were different in Vero cells namely; 1626 cm^{-1}, 1741 cm^{-1}, 2852 cm^{-1} 2923 cm^{-1}. Principal Component Analysis showed separation between the different types of cell death and the loadings plots indicated an increase in an additional band at 1623 cm^{-1} in dead cells. FTIR spectroscopy can be developed into an invaluable tool for the assessment of specific types of chemically induced cell death with notably different molecular signatures depending on whether the cells are cancerous and mechanism of cell death.

Keywords

FTIR spectroscopy, apoptosis, necrosis, flow cytometry, Transmission Electron Microscopy

[*] Corresponding author: Department of Biochemistry, University of Johannesburg, Auckland Park, Gauteng, South Africa. Fax: +27 11 559 4670; Tel: +27 11 559 2825; Email: dmeyer@uj.ac.za

1. Introduction

Cervical cancer, which is primarily caused by a sexually transmitted human papillomavirus (strains 16 and 18), is increasingly becoming a threat in low income countries. The stage, in which the disease is diagnosed, determines the type of treatment as well as the prognosis (Waggoner, 2003). The most successfully used drug for the treatment of cervical cancer is cisplatin, but resistant cancers support the development of improved alternatives (Florea and Busselberg, 2011). New chemotherapeutics derived from natural sources or through synthesis must be able to kill cancerous cells with the least amount of damage to neighbouring healthy cells and tissues. The assessment of new drug leads *in vitro*, uses label-based biochemical assays which assess the viability or death of cells by measuring different enzyme activities, biomarkers and cell morphologies during and after treatments (Le Roux et al., 2011; Stander et al., 2009).

Flow cytometry and transmission electron microscopy are routinely used for the assessment of cellular responses including cell death. In flow cytometry, cells are labelled with fluorescent markers, such as annexin-V and propidium iodide. Annexin-V binds to phosphatidylserine that is externalized on the plasma membrane during apoptosis. Propidium iodide intercalates into deoxyribonucleic acid (DNA)[†] when plasma membrane integrity is lost as in the case of necrosis (Vermes et al., 2000). Transmission electron microscopy (TEM) on the other hand is seen as the golden standard of characterizing the type of cell death induced. Using TEM cells are classified as apoptotic (with the presence or absence of autophagy) or necrotic based on morphological characteristics. In the case of necrosis, the plasma membranes are ruptured, mitochondria swollen with disruption of the cristae and nuclear dispersion visible. Characteristics of apoptosis, as seen with TEM, are associated with; plasma membrane blebbing, chromatin aggregation and detection of mitochondrial changes (Tinari et al., 2008).

[†] **Abbreviations:** FTIR – Fourier Transform Infrared, HeLa – cervical adenocarcinoma, Vero – African monkey kidney, FACS – Fluorescence Activated Cell Sorting, ANOVA – Analysis of Variance, DNA – Dioxyribonucleic acid, XTT - Sodium 3'-[phenyl amino-carbonyl)-3,4-tetrazolium]-bis-[4-methoxy-6-nitro) benzene sulfonic acid hydrate, PCA – Principal Component Analysis, PC – Principal Component, AE 76 - 2-(2-(diphenylphosphino) ethyl)pyridyl-gold(I) chloride, AE 125 - 2-(diphenylphosphino)-20-(N,N-dimethylamino) biphenylgold(I) chloride, CaF_2 – Calcium fluoride, PBS – Phosphate Buffered Saline, RT-CES – Real Time Cell Electronic Sensing, CST - Cytometer Setup and Tracking

Those mentioned above conventional biochemical assays require labels, costly instrumentation and can also be very labour intensive. New methods are under investigation for effectiveness in measuring cell death without the need for labels that are expensive and that can cross-react with other molecules. Two of those techniques are FTIR - and Raman spectroscopy. FTIR- and Raman spectroscopy have demonstrated biomedical applications in cancer research (Diem et al., 2012; Mantsch et al., 2002) including the ability to differentiate between healthy and cancerous cells / tissues, spectral differences between different tissues and types of cancers, grading of the stage of cancer progression and drug discovery where new drug leads were tested against the proliferation of cancerous cells as well as investigations on the molecular mechanism of action of known chemotherapeutics. Some spectral regions have been identified where cell death induction led to spectral differences in FTIR data (Gaudenzi et al., 2004; Holman et al., 2000; Jamin et al., 2003; Munro et al., 2010; Notingher et al., 2003). In this investigation, we set out to determine whether FTIR microspectroscopy could successfully distinguish between viable, apoptotic and necrotic cells.

2. Methodology

2.1 Cell death inducers and treatment of HeLa and Vero cells

Cervical carcinoma (HeLa) and African monkey kidney (Vero) cells (Highveld Biological, Johannesburg, South Africa) were used in this investigation. The selection of the cells were based on including both diseased (HeLa) and healthy (Vero) cells in this study because apoptosis and necrosis are universal processes that do not discriminate based on pathogenesis. The two cell lines are also morphologically similar. Propagation of the two cell lines was done as previously described (Le Roux et al., 2011). Cell death induction was facilitated by treatments previously confirmed to induce cytotoxic responses (le Roux et al., 2014). Two synthetic gold compounds namely; 2-(2-(diphenylphosphino) ethyl)pyridyl-gold(I) chloride (AE 76) and 2-(diphenylphosphino)-20-(N,N-dimethylamino) biphenylgold(I) chloride (AE125) were synthesized (Alcock et al., 1982; Calhorda et al., 2010) and characterized by Elkhadir (2014) (Elkhadir, 2014) under the supervision of Prof. Darkwa at the Department of Chemistry, University of Johannesburg, South Africa. Auranofin, a well-known gold compound notorious to be cytotoxic against cancer cells and used for the treatment of rheumatoid arthritis was included as a positive control. Necrosis

was induced by mechanical and chemical stress simultaneously through the use of ice cold methanol. Methanol is known to be extremely toxic to cells and when the cells (1.5 x 10^6 cells/mL) were exposed to ice cold methanol (2 mL), minuscule crystals caused poration of the plasma membranes. Cytotoxicity was measured with tetrazolium dye and confirmed with Real Time Cell Electronic Sensing (RT-CES) which indicated a decrease in cell viability within the first few hours after treatment for all apoptotic inducers (Le Roux, 2015).

When the cells reached 80-90% confluency, the cells were briefly trypsinized (Hyclone, Separations, Johannesburg) and counted. HeLa - and Vero cells were seeded in 10 mL complete media at 1.5 x 10^6 cells / 25 cm^2 flask and for the untreated control 0.2 x 10^6 cells / 25 cm^2 flask were plated. For downstream analysis of the cell, a minimum of 1.5 x 10^6 cells were essential and, therefore since sudden cytotoxic responses were seen with the treatments, 1.5 x 10^6 cells were plated initially. Due to the treatment time the cells doubled to ~ 1.5 x 10^6 cells/mL when 0.2 x 10^6 cells were plated. After 24 hours following cellular adherence to the cell culture flasks, the cells were exposed to the treatments (Table 1) and incubated for 72 hours. It was found that since the untreated cells were left to grow optimally for 96 hours in total, the cells reached approximately 1.5 x 10^6 cells in the flasks. To obtain a positive control for necrosis, cells were treated with 2 mL ice cold methanol (100%), for up to 10 minutes. After 72 hours, cells were harvested and suspended in complete media so the membranes could recover from trypsinization. The cells were then incubated for 1 hour in a humidified incubator at 37°C to allow the plasma membrane to recover. Cells (3 x 10^6) were centrifuged for 5 minutes at 1200 rpm. The supernatants were discarded and the cells washed with 2 mL binding buffer (BD Biosciences, Johannesburg, South Africa). The cells were then resuspended in 100 µL binding buffer and stained with 5 µL annexin-V and 5 µL propidium iodide (Apoptosis Detection Kit II, BDBioSciences, Johannesburg, South Africa). The cells were incubated for 15 minutes in the dark and washed with 500 µL binding buffer. The stained cells were suspended in 500 µL before flow cytometric analysis.

Table 1. Treatments used to induce maximum cell death in HeLa and Vero cells

Treatment	HeLa cells[a]	Vero cells[a]
Auranofin	5.6 µM	2.9 µM
AE 76	20.8 µM	13.2 µM
AE 125	17.8 µM	13.9 µM
Ice cold methanol	100%	100%

[a] **The concentrations used were determined by XTT to induce maximal cell death**

2.2 FACS staining and sorting for further analyses

Before sorting, standard protocols, as advised by BD Biosciences (Germany, Europe), were conducted. Those protocols included the calibration of the stream using the Accudrop delay function. After the stream had been calibrated, a test sort was done to determine the accuracy of the FACS sorting. The accuracy was tested using cytometer setup and tracking (CST) beads which gave three distinct populations of beads when interrogated. The beads were sorted in a two-way sort using the purity function. Approximately 40,000 beads per population were sorted before it was measured again. It was found that the sorting was always 99.99% accurate. The cells could not be analysed with the flow cytometer after sorting because the cells were photobleached and thus had no fluorescent signal. Annexin-V and propidium iodide fluorescence were measured using a BD FACS Aria flow cytometer (BD Biosciences) equipped with an air-cooled argon laser (excitation 488 nm). The annexin-V signal was detected using the FitC channel and the propidium iodide signal using the PE-Texas Red channel. The parameters of the FACS Aria (BDBiosciences, South Africa) were optimized for cell death analysis. Data of 10,000 cells were analysed with the BD FACS Diva Software Version 6.1 (BD Biosciences) before the sorting started. The population of interest (annexin-V negative, propidium iodide negative: viable cells or annexin-V positive, propidium iodide negative: early apoptotic cells or annexin-V negative, propidium iodide positive: necrotic cells) was sorted continuously until ~1.2 x 10^6 cells were sorted per population group of interest.

2.3 Transmission electron microscopy

After 3 x 10^6 cells were sorted, the cells were centrifuged for 5 minutes at 1200 rpm and resuspended in phosphate buffered saline (PBS). The supernatants were discarded without disruption of the pellets and the cells fixated in TEM fixative (2.5% glutaraldehyde, 2.5% formaldehyde in 0.075 M PBS, pH 7.4) for 1 hour. The samples were rinsed with 0.075 M PBS twice for 10 minutes each and then fixed in 0.5% aqueous osmium tetroxide for 30 minutes. After incubation, the samples were rinsed twice with distilled water. The samples were then dehydrated stepwise with ethanol (30%, 50%, 70%, 90%, 100%, 100%, 100% each for 10 minutes) and stored at 4°C for a few days until all the samples were sorted and dehydrated. The dehydrated samples were infiltrated with 50% Quetol for 30 minutes, followed by 100% Quetol for 3 hours. After infiltration, the samples were polymerized at

60°C for 40 hours. Ultrathin sections of the samples were cut with a Reichert-Jung Ultracut E microtome with a Diatome diamond knife and transferred onto copper mesh grids. The sections were contrasted by staining the samples with 4% uranyl acetate for 5 minutes, followed by staining the samples with Reynold's lead citrate for 2 minutes (Van der Merwe and Coetzee, 1992). The sections were then examined using a multipurpose transmission electron microscope (Phillips, 301) at the Laboratory of Microscopy and Microanalysis (University of Pretoria, South Africa) (Venter et al., 2014).

2.4 FTIR microspectroscopy analyses of sorted cells

Sorted cells were incubated at room temperature in 1 mL 10% formalin (in PBS) for 10 minutes. The supernatant was discarded and the cells washed twice with 1 mL sterile distilled water to remove all traces of formalin and PBS, which could influence the spectra. The supernatant was removed and the cells suspended in 10 µL sterile distilled water. The cell suspensions (3 µL) were dried in the biosafety hood for one hour on sterile CaF_2 discs. The FTIR spectra were obtained with a 15x IR objective of Hyperion microscope attached to a Bruker V70x spectrometer equipped (Bruker, Germany). Using a liquid nitrogen cooled detector connected to the microscope, 30 areas were analysed containing a lawn of cells (~ 400 cells per area). Spectra in the range of 850-4000 cm^{-1} were recorded. Data were collected in transmission mode and spectra (4 cm^{-1} spectral resolution, co-added for 100 scans) recorded using Bruker OPUS software. All the spectra were pre-processed using OPUS 7 software. Atmospheric contributions (water vapour and CO_2) were subtracted and the spectra vector normalized. Baseline correction was done using the rubber band function. Second derivatives were calculated (17 smoothing points) and used for interpretation and statistical analysis (le Roux et al., 2015; Machana et al., 2012; Zelig et al., 2009). An unsupervised method, hierarchical cluster analysis was performed to identify trends in the spectra. One way ANOVA was calculated for all bands together with the Tukey and Bonferroni posthoc tests to identify significantly different ($p < 0.05$) bands. HeLa cells were analysed and trends were observed with natural product induced or gold complex induced apoptosis and necrosis. The trends were noted when the positive control, as well as the experimental treatments, were significantly altered. After the bands had been identified in HeLa cells, the bands were also investigated for Vero cells to determine if there were any shared cell death marker bands.

3. Results

HeLa and Vero cells were sorted to obtain pure populations of cells that were either viable, apoptotic or necrotic. To confirm the staining and sorting, the cells were investigated using transmission electron microscopy before further analyses with FTIR spectroscopy. With flow cytometry, it was observed that untreated cells were viable and thus remained unstained, early apoptotic cells (such as treated with the positive control, auranofin) stained positively with annexin-V, while necrotic cells (treated with methanol) were positively stained with propidium iodide. The same trend was seen irrespectively of the type of cell line (Fig. 1 and Fig 2).

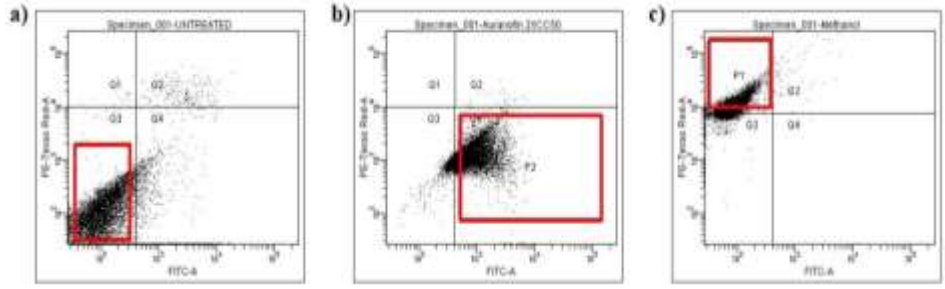

Fig. 1. Representative dot plots used to select an area of interest within the cell population (HeLa cells) to be sorted. Typical dot plots for sorting (a) viable cells (annexin-V negative, propidium iodide negative), (b) apoptotic cells (annexin-V positive, propidium iodide negative) or (c) necrotic cells (annexin-V negative, propidium iodide positive).

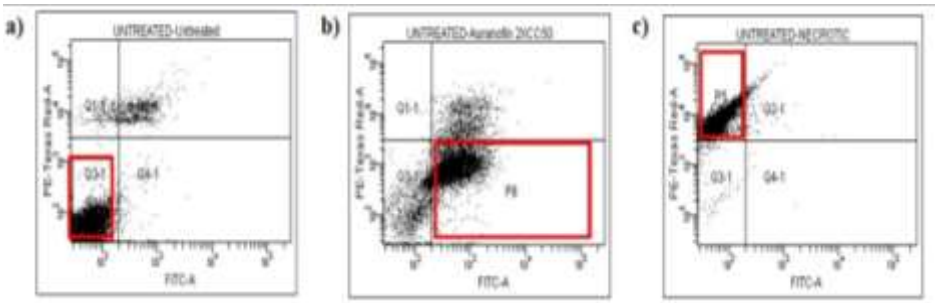

Fig. 2. Representative dot plots used to select an area of interest within the cell population (Vero cells) to be sorted. Typical dot plots for sorting (a) viable cells, (b) apoptotic cells or (c) necrotic cells. The trend was the same as was found in HeLa cells.

To confirm that the sorting process could effectively separate populations of interest, transmission electron microscopy was performed on collected populations. It was found that untreated viable cells (annexin-V negative, propidium iodide negative) had average nuclear

material distribution within the nucleus and a clearly defined nucleolus while the nuclear envelope was intact and clearly visible. The organelles were plentiful and cytoplasm densities were similar between the two cell lines. The plasma membranes were intact with normally distributed protrusions seen, usually used for adherence (Fig. 3 (a) and Fig. 4 (a)). Necrotic sorted cells were achieved by treating the cells with ice cold methanol. It was clear that the sorted cells had damaged plasma membranes and aggregated cellular components. Severely damaged mitochondria were observed which included swollen mitochondria with disrupted cristae. The nuclear material was also dispersed and granular (Fig. 3 (b) and Fig. 4 (b)). Cells that were sorted as early apoptotic mostly showed signs of condensed chromatin that in most cases were fragmented and marginalized on the inside of the nuclear envelope. Big clear vacuoles were present in most apoptotic cells. Different severities of apoptosis were identified (Fig .3 (c - e) and Fig. 4 (c - e)).

Fig. 3. Electron micrographs of the sorted HeLa cells based on annexin-V and propidium iodide staining. (a) Untreated viable cell with a large nucleus (red arrow) and intact plasma membrane (purple arrow), (b) the methanol treated necrotic cell had a ruptured plasma membrane (purple arrow), dispersed granular nuclear material (red arrow) and swollen mitochondria (green arrow) in the cytoplasm associated with necrosis, (c) auranofin treated cell showed signs of apoptosis, which includes a nucleus with condensed chromatin (red arrow), membrane blebbing (purple arrow), big vacuoles (blue arrow) and apoptotic bodies (black arrow), (d) AE76 treated cell showed signs of nuclear membrane folds (red arrow), vacuoles (blue arrow) and plasma membrane blebbing (purple arrow) with apoptotic bodies (black arrow), (e) AE 125 treated cell has nuclear membrane folds (red arrow), plasma membrane blebbing (purple arrow) with apoptotic bodies (black arrow).

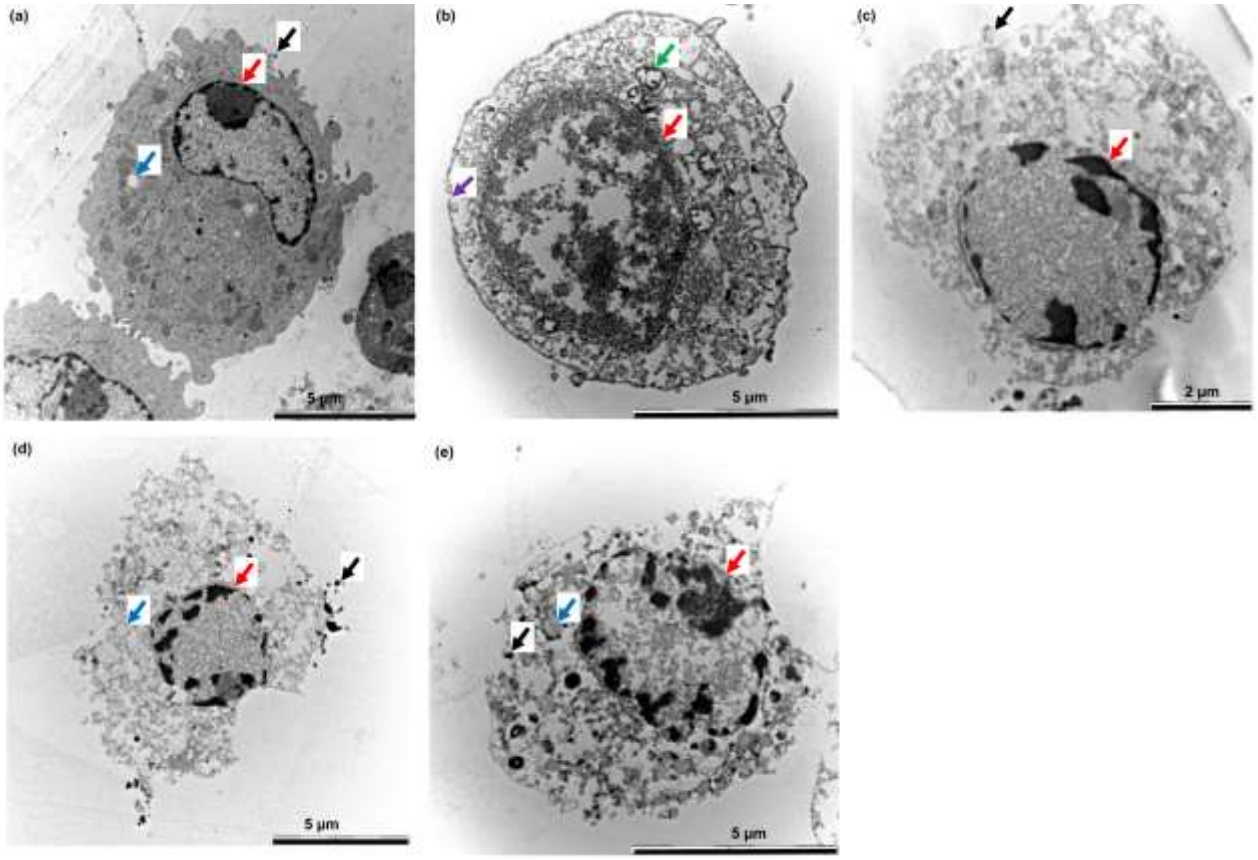

Fig. 4. Electron micrographs of the sorted Vero cells based on annexin-V and propidium iodide staining. (a) Untreated viable cell with intact plasma membrane (purple arrow) and nucleus (red arrow) with a vacuole (blue arrow), b) methanol treated necrotic cell showed severe morphological damage due to chemical stress like ruptured plasma membrane (purple arrow) and a nucleus containing aggregated dispersed chromatin. Mitochondria were swollen and contained disrupted cristae. (c) Auranofin treated cell had marginalised nuclear material (red arrow) with apoptotic bodies being released from the blebbing plasma membrane (black arrow). (d) AE76 treated cells had fragmented condensed chromatin (red arrow) with vacuoles present in the cytoplasm (blue arrow) and visible apoptotic bodies (black arrow), while (e) AE 125 treated cells has similar apoptotic features as AE 76 treated cells. The features include fragmented DNA and apoptotic bodies.

3.1 FTIR spectroscopy measurements for the detection of cell death specific vibrational bands

After the confirmation that the cells were successfully sorted into viable, apoptotic and necrotic cell death groups using TEM, FTIR spectroscopy was used to investigate if the same vibrational bands of apoptosis and necrosis were evident when using different cell death inducers and different cell lines. The second derivatives of FTIR spectra were used for the interpretation of the results. After the data had been analysed, it was found that a definite trend existed in most of the spectral bands. The trend was based on the fact that viable cells' spectra were significantly different when compared to apoptotic - and necrotic cells' spectra. Significantly ($p < 0.05$, one way ANOVA, post hoc tests) altered bands were identified and the similarities and differences between the cell lines listed (Fig. 5, Fig. 6 and Table 2).

Based on significant changes in both cell lines four bands were identified which could discriminate between viable and necrotic cells namely 989 cm^{-1}, 2852 cm^{-1}, 2875 cm^{-1} and 2923 cm^{-1} (Table 2). None of these or any other bands could distinguish between viable and apoptotic cells for positive controls or experimental treatments. Four bands could distinguish necrotic cells from apoptotic cells in both cell lines these were; 1741 cm^{-1}, 2852 cm^{-1}, 2875 cm^{-1} and 2923 cm^{-1}. Only one band in HeLa cells could distinguish between viable and gold complex induced apoptosis (1294 cm^{-1}). Nine bands were identified as able to make a distinction between viable and necrotic HeLa cells. Those bands were 933 cm^{-1}, 970 cm^{-1}, 989 cm^{-1}, 1091 cm^{-1}, 1238 cm^{-1}, 2852 cm^{-1}, 2875 cm^{-1}, 2923 cm^{-1}. Eight bands could also distinguish between viable and necrotic Vero cells (1022 cm^{-1}, 1315 cm^{-1}, 1346 cm^{-1}, 1718 cm^{-1}, 2852 cm^{-1}, 2875 cm^{-1}, 2896 cm^{-1} and 2923 cm^{-1}). Four bands were identified to be significantly different between viable and gold complex induced apoptosis in Vero cells namely; 1626 cm^{-1}, 1741 cm^{-1}, 2852 cm^{-1} 2923 cm^{-1}. Significantly altered bands that could discriminate between necrotic and apoptotic Vero cells were; 989 cm^{-1}, 1022 cm^{-1}, 1626 cm^{-1}, 1718 cm^{-1}, 1741 cm^{-1}, 2852 cm^{-1}, 2875 cm^{-1}, 2896 cm^{-1} and 2923 cm^{-1}.

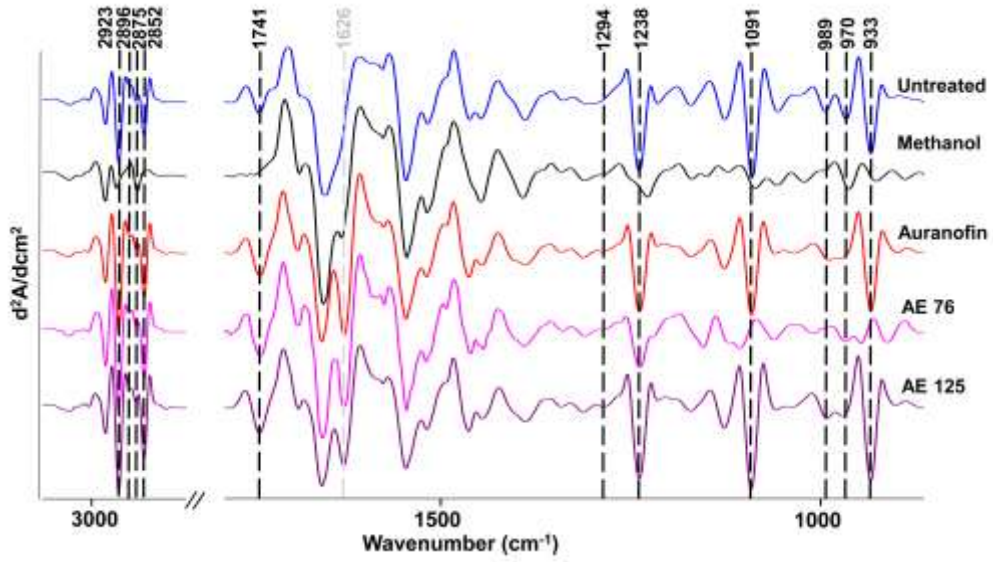

Fig. 5. The average second derivatives of untreated (viable) – and treated HeLa cells. Viable cells were compared to methanol treated cells (necrotic) as well as to synthetic (auranofin, AE 76 and AE 125) gold compounds treated cells. Although some of the spectral trends were visible to the naked eye, statistical analyses were conducted to determine significantly altered bands. Significantly different bands (ANOVA one way, posthoc Tukey and Bonferonni, $p < 0.05$) are indicated in black while the band indicated in grey showed visible evidence of cell death which was not significant.

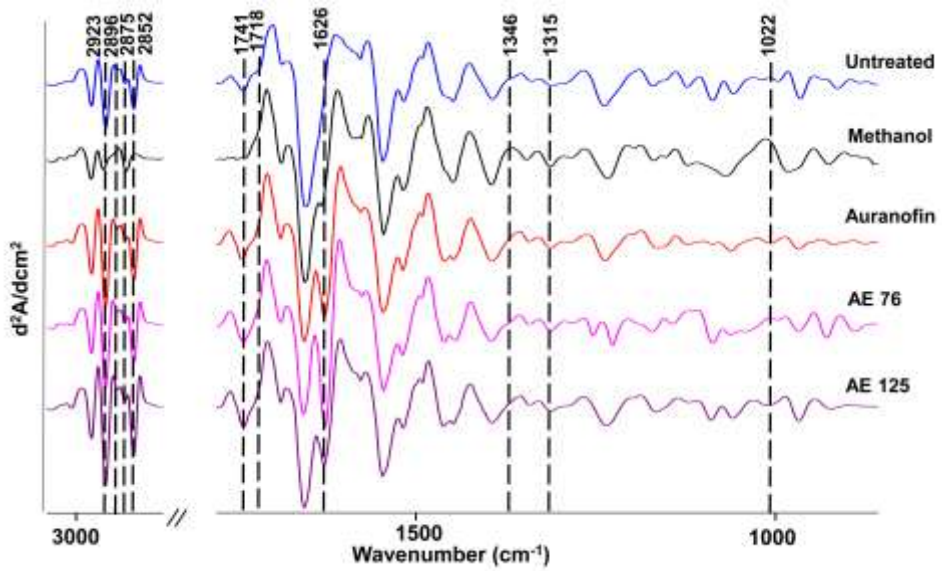

Fig. 6. The average second derivatives of untreated (viable) – and treated Vero cells. Viable cells were compared to synthetic (auranofin, AE 76 and AE 125) gold compounds treated cells and methanol treated (necrotic) cells. Although some of the spectral alterations were visible to the naked eye, statistical analyses were conducted to determine significantly altered bands. Significantly different bands (ANOVA one way, posthoc Tukey and Bonferonni, $p < 0.05$) are indicated in black.

Table 2. A summary of the significantly ($p < 0.05$, One way ANOVA and post hoc tests) altered FTIR bands and the description of the alterations in terms of viability and cell death.

Wavenumber	p-value (HeLa)	Post hoc[3]	p-value (Vero)	Post hoc
933	0.0004	Viable versus necrosis	NS[4]	
970	0.009	Viable versus necrosis	0.001	NS
989	0.004	Viable versus necrosis	0.0002	Viable versus necrotic Necrotic versus apoptotic
1022	0.03	NS	0.003	Viable versus necrotic Necrosis versus apoptosis (GC)[5]
1091	0.002	Viable versus necrosis	NS	
1238	0.009	Viable versus necrosis	NS	
1294	0.005	Viable versus apoptosis (GC)	NS	
1315	0.03	NS	0.0004	Viable versus necrotic
1346	NS		0.009	Viable versus necrotic
1626	NS		0.00004	Viable versus apoptosis (GC) Apoptosis versus necrotic Viable versus necrotic
1718	NS		0.0001	Viable versus necrosis Necrosis versus apoptosis (GC)
1741	0.004	Necrosis versus apoptosis (GC)	0.00009	Viable versus necrosis Viable versus apoptosis (GC) Necrosis versus apoptosis (GC)
2852	0.002	Viable versus necrosis Necrosis versus apoptosis (GC)	< 0.0001	Viable versus necrosis Viable versus apoptosis (GC) Necrosis versus apoptosis (GC)
2875	0.0003	Viable versus necrosis Necrosis versus apoptosis (GC)	0.0005	Viable versus necrosis Necrosis versus apoptosis (GC)
2896	0.025	NS	0.0002	Viable versus necrosis Necrosis versus apoptosis (GC)
2923	0.0004	Viable versus necrosis Necrosis versus apoptosis (GC)	< 0.0001	Viable versus necrosis Viable versus apoptosis (GC) Necrosis versus apoptosis (GC)

[3] Tukey test followed by Bonferroni test where $p < 0.05$

[4] NS indicates to Not Significant

[5] GC refers to gold complexes; auranofin (positive control), AE 76 and AE 125.

3.2 Principal component analysis of FTIR spectra

Principal component analysis (PCA) was carried out for all the treatments to determine the patterns in the spectral data based on similarities and differences between the data. This analysis is an unsupervised method used for data reduction (Ellis and Goodacre, 2006). It was found that when all of the HeLa cells' data were analysed in one PCA, there was good separation. Significant band alterations were also found to be extremely variant between cell lines. Since the PCA was performed on second derivatives, a negative score was associated with a positive loading (Munro et al., 2010). When the HeLa cells were treated with metallodrugs, some separation could also be observed which signifies that FTIR spectroscopy can distinguish between different types of cell death induction. The first two PCs explained the total variance within the spectra (Fig. 7, 8 (a)) and altered bands mostly responsible for the separation were indicated in Fig. 7, 8 (b).

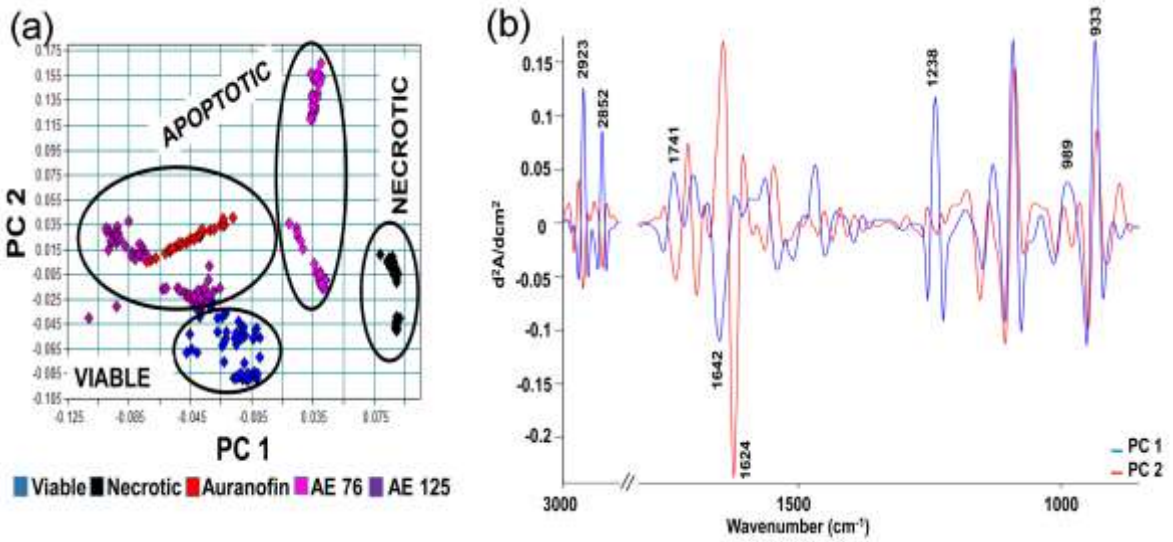

Fig. 7. (a) The PCA plot of viable, necrotic and metallodrug induced apoptosis. Clear separation was seen between viable / apoptotic and necrotic HeLa cells in PC 1 while PC 2 moderately separated the viable cells from apoptotic- and necrotic cells. It was observed that AE 125 treated cells were situated very closely to the viable cells. **(b) The loading plots of the PCA.** The major differences indicated was also determined to be in most cases significantly different.

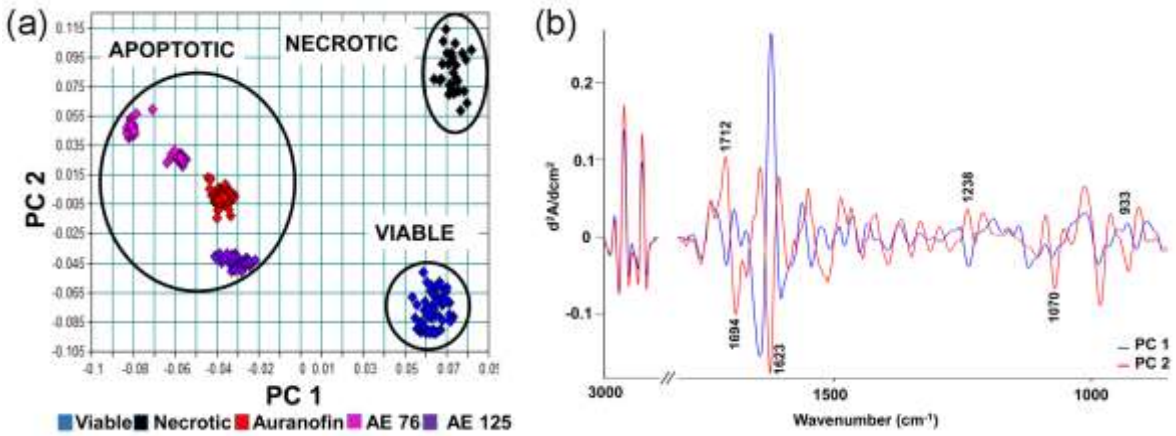

Fig. 8. (a) The PCA plot of viable, necrotic and metallodrug induced apoptosis in Vero cells. Clear separation was seen between viable / necrotic and apoptotic cells in PC 1 while PC2 separated the viable cells from apoptotic- and necrotic cells. **(b) The loading plots of the PCA.** The major differences indicated was also determined to be in most cases significantly different.

Discussion

Transmission electron microscopy was performed on collected populations. Sorted unstained HeLa and Vero cells showed ultrastructural characteristics of unstressed cells that were viable. Ice cold methanol (necrosis inducer) contained small ice crystals that porated the plasma membranes of treated cells, causing the cell contents to leak. Severely damaged mitochondria were observed which included swollen mitochondria with disrupted cristae that were caused by the methanol being extremely toxic to cells and led to the denaturation of proteins. The nuclear material was also dispersed and granular which could have been due to the denaturing of nucleic acids exposed to 100% methanol. Early apoptotic cells had characteristic signs of condensed chromatin and big clear vacuoles. Condensed chromatin and fragmentation had been linked to the early stage of apoptosis and even the "point of no return" for dying cells (Elmore, 2007; Kroemer et al., 2009). Since apoptosis is a dynamic process, the morphological characteristics differed between the treatments depending on the onset time of cell death induction. The probability of interrogating the correct type of induced cell death, using FTIR spectroscopy was high because of the accuracy of sorting.

The second derivatives of FTIR spectra were used for the interpretation of the results since second derivatives are known to emphasize small spectral differences (Machana et al., 2012;

Zelig et al., 2009). Firstly in HeLa cells, the band at 933 cm^{-1} was assigned to the vibrational mode of the C-O-C ring of deoxyribose in Z-form DNA (Banyay et al., 2003; Ghomi et al., 1990; Movasaghi et al., 2008). The bands at 989 cm^{-1}, 1238 cm^{-1} and 1091 cm^{-1} were assigned to PO_4^{2-} (nucleic acids), antisymmetric and symmetric stretching modes of phosphates (PO_2^-) found in DNA (Barth et al., 1995; de la Fuente et al., 2004; Mohlenhoff et al., 2005).

The presence of the five above mentioned bands in viable cells were indicative that the nuclei were associated with metabolically active cells. The high absorbance at 933 cm^{-1} could be indicative of active transcription in which case Z-DNA could be prominent (Rich and Zhang, 2003), while on the other hand, the cells might have been moderately stressed due to the sorting process which could also have increased the peak absorbance or it could be due to dehydration of the cells. In a previous study it was found that viable unsorted HeLa cells only had a very small shoulder band at 933 cm^{-1}, while chemically stressed cells had a prominent band at 933 cm^{-1} (le Roux et al., 2015), therefore supporting the statement that the viable cells in this study might have been experiencing some minor mechanical/electrical stress due to the sorting process. Dehydration of the cells was also not likely to have caused in increase in this peak, since drying time of the cells remained the same in this and the previous study (le Roux et al., 2015).

On the other hand the TEM micrographs of sorted viable HeLa cells did not indicate any visible signs of the cells experiencing possible fatal stress and therefore the cells were prone to be more metabolically active due to the small amount of cellular stress (Barteneva et al., 2013; le Roux et al., 2015). Strong DNA signals are usually detected in metabolically active cells or in cells that are in late stages of apoptosis when the cell's DNA became fragmented. The detection of DNA signals is very low when the DNA is condensed and tightly packed (Mohlenhoff et al., 2005). In the case of auranofin and AE 125 treated HeLa cells, the prominent bands at 933 cm^{-1}, 1091 cm^{-1} and 1238 cm^{-1} could be indicative of DNA fragmentation that was also evident in the TEM micrographs. AE 76 treated apoptotic cells had low absorbencies for 933 cm^{-1}, 989 cm^{-1}, 1091 cm^{-1} and 1238 cm^{-1} compared to viable cells, which could be due to later stages of apoptosis, where the nucleus membranes become affected and starts blebbing, while the formation of apoptotic bodies could also lead to lower

concentrations of DNA in the cell. Necrotic HeLa cells displayed faint bands at 933 cm^{-1}, 989 cm^{-1}, 1091 cm^{-1} and 1238 cm^{-1} which was as expected due to the dispersion of DNA in the nucleus and lysis of the nuclear membrane (karyolysis).

Another DNA related band that changed significantly in HeLa cells was 1294 cm^{-1} assigned to N-H vibrations of cytosine (Movasaghi et al., 2008). The vibrational band increased significantly when the cells were treated with gold compounds. This increase in absorbance could be due to interactions with the gold compounds or the mechanism elicited with this type of compounds such as DNA fragmentation or an interaction of nucleic acids exposing cytosine. An increase in phosphorylated proteins and DNA (970 cm^{-1}) were detected in all treated HeLa cells but were only found be significantly increased in necrotic cells, which could be due to a survival mechanism of cells containing DNA breaks (Didenko et al., 2003) in which case repair proteins were phosphorylated before trying to fix the breaks (Summers et al., 2011). None of those mentioned above vibrational bands, except for 989 cm^{-1}, were significantly altered in Vero cells after treatment, although similar trends between the treatments were seen in some of the bands (Fig. 6).

Glycogen (1022 cm^{-1}) was significantly decreased in necrotic Vero cells. Necrosis is a passive process and thus does not need energy for progress, but since the plasma membranes were ruptured due to the treatment, it was most likely that the metabolites leaked out of the cells. In Vero cells, the vibrational bands at 1315 cm^{-1} and 1346 cm^{-1} were altered in necrotic cells that led to an increase in the intensity of the bands. The bands were assigned to CH vibrations and protein bound tryptophan respectively. Due to the harsh methanol treatment that the cells underwent many of the proteins could have denatured. One of the vibrational bands visibly altered in both dead HeLa - and Vero cells (but only significantly altered in Vero cells) was the appearance of the band at 1626 cm^{-1}. This band was assigned to intermolecular β-sheet protein-protein interactions suggestive of protein compactness and the degree of protein aggregation (Doglia et al., 2008). Zelig *et al.* (2009) found that a decrease in α-helices and an increase in β-sheets were indicative of apoptosis and that the degree of β-sheets could be linked to the stage of apoptosis (Zelig et al., 2009). In the present study, it was observed that all apoptotic HeLa and Vero cells had similar trends in the presence of β-sheets. Recently, Yadav *et al.* (2014) found that mitochondrial proteins were favourably in β-

sheets as compared to α-helices during apoptosis (Yadav et al., 2014), which may partly explain the detection of β-sheets in apoptotic cells. Necrotic HeLa and Vero cells also had detectable conformational changes in amide I region, with an increase in β-sheets, although not as prominent as found with apoptotic cells. The β-sheet formation could be due to the severity of the necrosis inducer used in the present study and therefore, the possibility of detecting this band after other types of necrotic induction should be investigated. In this study, the detection of β-sheets was indicative of cell death and not particularly apoptosis.

A very small shoulder band was identified at 1718 cm^{-1} and assigned to guanine and thymine (C=O) (Dovbeshko et al., 2000) as well as glutamine and asparagine in Vero cells. This band was detected as significantly altered only in Vero cells. It was seen that the small band decreased in necrotic cells. The change within the peak suggests changes within DNA and RNA most likely due to the dispersion of the nuclear material. The vibrational bands at 1464 cm^{-1} (CH_2 vibration of acyl chain of lipids), 1741 cm^{-1} (C=O ester vibration of phospholipids), 2852 cm^{-1} (symmetric CH_2 vibration of lipids), 2875 cm^{-1} (C-H stretching of lipids and proteins of CH_3) and 2923cm^{-1} (antisymmetric CH_2 vibrations of lipids) (Miller and Dumas, 2010; Movasaghi et al., 2008; Munro et al., 2010; Zelig et al., 2009) were altered in both cell lines. The vibrational band of necrotic HeLa cells at 1741 cm^{-1} were significantly lower in absorbencies as compared to apoptotic cells but not compared to viable cells. This decrease in lipid absorbance could be due to some of the lipid components (lipophilic) of the cells having dissolved/extracted in the methanol during treatment. The vibrational bands 2852 cm^{-1}, 2875 cm^{-1} and 2923 cm^{-1} were significantly affected by the induction of necrosis; with necrotic cells being significantly different from viable and apoptotic cells.

A possible reason why viable and apoptotic cells were not significantly different may be due to the fact that when cells undergo apoptosis, the plasma membranes remain intact (Kepp et al., 2011), while with chemically induced necrosis, the plasma membrane structural integrity is compromised, causing some lipids to dissolve in the methanol. Similar trends such as the disappearance of the peaks at 2925 cm^{-1} and 2852 cm^{-1} were seen when Vero cells were fixed using acetone (Hastings et al., 2008). Gaudenzi *et al.* (2004) found a positive correlation between the vibrational band of ~2928 cm^{-1} increasing in intensity and the detection of the % apoptosis using annexin-V. Annexin-V binds to phosphatidylserine, which is a phospholipid

externalized during apoptosis. It was speculated by Gaudenzi *et al.* (2004) that the vibrational band could be directly attributed to phosphatidylserine (Gaudenzi et al., 2004). These authors used Jurkat cells treated with actinomycin D while, in the current study, various treatments tested on different cell lines showed highly variable spectral intensities of 2928 cm^{-1} with no significant differences observed for this band. The region of 2800 – 3000 cm^{-1} could be useful in distinguishing necrotic cells from viable cells or necrotic cells from apoptotic cells. A vibrational band around 1742 cm^{-1} assigned to C=O (ester linkage) of membrane phospholipids was identified with major spectral changes accompanied by different types of induced cell death. Under normal conditions, when cells are proliferating, only a shoulder of this peak can be seen (Matthaus et al., 2006; Munro et al., 2010). Munro *et al.* (2010) investigated the cytotoxicity of arsenic trioxide against the proliferation of leukemic HL60 cells and tried to characterize the changes in the 1740 cm^{-1} band to apoptosis with little success, since trypan blue enters dead cells and does not discriminate between apoptotic and necrotic cells. Holman *et al.* (2000) acknowledged the potential of the phospholipid peak as a possible molecular marker for dead cells (Holman et al., 2000). On the other hand, other researchers concluded that lipid content in terms of relative absorbance cannot be used for distinction between types of cell deaths (Jamin et al., 2003; Zelig et al., 2009). In the PCA analysis, the most prominent band was identified as an increase in β-sheets in the amide I band which was associated with dead cells. In the loading plot, it was confirmed that significantly altered bands (Table 2) were mostly responsible for the separation seen in Fig. 8 (b).

To summarize, in this investigation pure populations (viable, apoptotic and necrotic) were obtained by FACS. Successful sorting was confirmed by TEM after which populations were investigated using FTIR microspectroscopy. Several bands were found to be useful in distinguishing between necrotic and viable cells in different cell lines. This study demonstrated the importance of investigating cancer cells in parallel with noncancerous cells when assessing the particular type of cell death induced by a drug lead. The conformational change in the amide I, with a definite increase in β-sheets, is of importance and could be developed into a biomarker of cell death, although the exact origin of the band should still be further analysed. Lipid rich regions were also detected as potential parameters for cell death detection. DNA rich regions of the FTIR spectra were found to be of interest in cancerous cells, with many bands changing significantly when cell death was induced. FTIR

spectroscopy can be developed into an invaluable tool to investigate new drug leads and to study the repurposing of drugs conventionally used to treat other diseases (for example auranofin).

Acknowledgements

The authors would like to acknowledge the following organizations for funding this project; the University of Pretoria, the Technology Innovation Agency (TIA) and the National Research Foundation (NRF) of South Africa. The authors would also like to acknowledge the technical assistance provided by Dr. Smit at the Flow Cytometry Unit (Department of Biochemistry, University of Pretoria) and Mr. Chris van der Merwe and Ms. Antoinette Buys of the Microanalysis Unit (University of Pretoria) for their technical assistance during TEM analysis.

4. References

Alcock, N.W., Moore, P., Lampe, P.A., Mok, K.F., 1982. Crystal and Molecular Structures of Two Complexes of Diphenyl(2- pyridy1)phosphine (L): [AuCIL] and [Ag2C12L,]. Dalt. Trans. 207–210.

Banyay, M., Sarkar, M., Graslund, A., 2003. A library of IR bands of nucleic acids in solution. Biophys. Chem. 104, 477–488. doi:10.1016/S0301-4622

Barteneva, N.S., Ketman, K., Fasler-Kan, E., Potashnikova, D., Vorobjev, I.A., 2013. Cell sorting in cancer research--diminishing degree of cell heterogeneity. Biochim. Biophys. Acta 1836, 105–122. doi:10.1016/j.bbcan.2013.02.004

Barth, A., Hauser, K., Mantele, W., Corrie, J.J.E.T., Trenthams, D.R., 1995. Photochemical Release of ATP from "Caged ATP" Studied by Time-Resolved Infrared Spectroscopy. J. Am. Chem. Soc. 117, 10311–10316.

Calhorda, M.J., Ceamanos, C., Crespo, O., Gimeno, M.C., Laguna, A., Larraz, C., Vaz, P.D., Villacampa, M.D., 2010. Heteropolynuclear gold complexes with metallophilic interactions: modulation of the luminescent properties. Inorg. Chem. 49, 8255–8269. doi:10.1021/ic100413x

De la Fuente, M., Hernanz, A., Navarro, R., 2004. IR and Raman study on the interactions of the 5'-GMP and 5'-CMP phosphate groups with Mg(II), Ca(II), Sr(II), Ba(II), Cr(III), Co(II), Cu(II), Zn(II), Cd(II), Al(III) and Ga(III). J. Biol. Inorg. Chem. 9, 973–986. doi:10.1007/s00775-004-0593-5

Didenko, V. V, Ngo, H., Baskin, D.S., 2003. Early Necrotic DNA Degradation. Am. J. Pathol. 162, 1571–1578.

Diem, M., Miljkovic, M., Bird, B., Chernenko, T., Schubert, J., Marcsisin, E., Mazur, A., Kingston, E., Zuser, E., Papamarkakis, K., Laver, N., 2012. Applications of Infrared and Raman Microspectroscopy of Cells and Tissue in Medical Diagnostics : Present Status and Future Promises. Spectrosc. An Int. J. 27, 463–496. doi:10.1155/2012/848360

Doglia, S.M., Ami, D., Natalello, A., Gatti-Lafranconi, P., Lotti, M., 2008. Fourier transform infrared spectroscopy analysis of the conformational quality of recombinant proteins within inclusion bodies. Biotechnol. J. 3, 193–201. doi:10.1002/biot.200700238

Dovbeshko, G.I., Gridina, N.Y., Kruglova, E.B., Pashchuk, O.P., 2000. FTIR spectroscopy studies of nucleic acid damage. Talanta 53, 233–246.

Elkhadir, A.Y.F., 2014. Phosphorous-nitrogen gold (I), palladium (II) and platinum (II) bimetallic complexes as potential antimalaria, antiHIV, antimycobateria, and anticancer agents. University of Johannesburg.

Ellis, D.I., Goodacre, R., 2006. Metabolic fingerprinting in disease diagnosis: biomedical applications of infrared and Raman spectroscopy. Analyst 131, 875–885. doi:10.1039/b602376m

Elmore, S., 2007. Apoptosis: A review of programmed cell death. Toxicol. Pathol. 35, 495–516. doi:10.1080/01926230701320337

Florea, A.-M., Busselberg, D., 2011. Cisplatin as an Anti-Tumor Drug: Cellular Mechanisms of Activity, Drug Resistance and Induced Side Effects. Cancers (Basel). 3, 1351–1371. doi:10.3390/cancers3011351

Gaudenzi, S., Pozzi, D., Toro, P., Silvestri, I., Morrone, S., Castellano, A.C., 2004. Cell apoptosis specific marker found by Fourier Transform Infrared Spectroscopy. Spectroscopy 18, 415–422.

Ghomi, M., Leterllier, R., Liquier, J., Taillandier, E., 1990. Interpretation of DNA vibrational spetra by normal coordinate analysis. Int. J. Biochem. 22, 691–699.

Hastings, G., Wang, R., Krug, P., Katz, D., Hilliard, J., 2008. Infrared microscopy for the study of biological cell monolayers. I. Spectral effects of acetone and formalin fixation. Biopolymers 89, 921–930. doi:10.1002/bip.21036

Holman, H., Martin, M., Blakely, E., Bjornstad, K., McKinney, W., 2000. IR spectroscopic characteristics of cell cycle and cell death probed by synchrotron radiation based Fourier transform IR spectromicroscopy. Biopolym. 57, 329–335.

Jamin, G.E., Miller, L., Moncuit, J., Fridman, W., Dumas, P., Teillaud, J., 2003. Chemical heterogeneity in cell death: Combined synchrotron IR and fluorescence microscopy studies of single apoptotic and necrotic cells. Biopolym. 72, 366–373.

Kapewangolo, P., 2013. Investigating plant species from the Lamiaceae family for activity against HIV/AIDS and immunomodulatory properties. University of Pretoria.

Kepp, O., Galluzzi, L., Lipinski, M., Yuan, J., Kroemer, G., 2011. Cell death assays for drug discovery. Nat. Rev. - Drug Discov. 10, 221–237. doi:10.1038/nrd3373

Kroemer, G., Galluzzi, L., Vandenabeele, P., Abrams, J., Almeri, E., Baehrecke, E., Blagosklonny, M., El-Deiry, W., Golstein, P., Green, D., Hengartner, M., Knight, R., Kumar, S., Lpipon, S., 2009. Classification of cell death. Cell death Differ. 16, 3–11. doi:10.1038/cdd.2008.150.

Le Roux, K., 2015. Comparing biochemical and biophysical methodologies for the characterization of induced cell death. University of Pretoria.

Le Roux, K., Hussein, A.A., Lall, N., 2011. In vitro chemo-preventative activity of Crotalaria agatiflora subspecies agatiflora Schweinf. J. Ethnopharmacol. 138, 748–755. doi:10.1016/j.jep.2011.10.011

Le Roux, K., Prinsloo, L.C., Meyer, D., 2014. Metallodrug induced apoptotic cell death and survival attempts are characterizable by Raman spectroscopy. Appl. Phys. Lett. 105, 123702. doi:10.1063/1.4896616

Le Roux, K., Prinsloo, L.C., Meyer, D., 2015. Cellular injury evidenced by impedance technology and infrared microspectroscopy. Spectrochim. Acta Part A Mol. Biomol. Spectrosc. 138, 321–330. doi:10.1016/j.saa.2014.11.089

Machana, S., Weerapreeyakul, N., Barusrux, S., Kanjana, T., Tanthanuch, W., 2012. FTIR microspectroscopy discriminates anticancer action on human leukemic cells by extracts of Pinus kesiya; Cratoxylum formosum ssp. pruniflorum and melphalan. Talanta 93, 371–382. doi:10.1016/j.talanta.2012.02.058

Mantsch, H.H., Choo-Smith, L.-P., Shaw, R.A., 2002. Vibrational spectroscopy and medicine: an alliance in the making. Vib. Spectrosc. 30, 31–41.

Matthaus, C., Boydston-White, S., Miljkovic, M., Romeo, M., Diem, M., 2006. Raman and Infrared Microspectral Imaging of Mitotic Cells. Appl. Spectrosc. 60, 1–8.

Miller, L.M., Dumas, P., 2010. From structure to cellular mechanism with infrared microspectroscopy. Curr. Opin. Struct. Biol. 20, 649–656. doi:10.1016/j.sbi.2010.07.007

Mohlenhoff, B., Romeo, M., Diem, M., Wood, B.R., 2005. Mie-Type Scattering and Non-Beer-Lambert Absorption Behavior of Human Cells in Infrared Microspectroscopy. Biophys. J. 88, 3635–3640. doi:10.1529/biophysj.104.057950

Movasaghi, Z., Rehman, S., ur Rehman, D.I., Rehman, I., 2008. Fourier Transform Infrared (FTIR) spectroscopy of biological tissues. Appl. Spectrosc. Rev. 43, 134–179. doi:10.1080/05704920701829043

Munro, K.L., Bambery, K.R., Carter, E.A., Puskar, L., Tobin, M.J., Wood, B.R., Dillon, C.T., 2010. Synchrotron radiation infrared microspectroscopy of arsenic-induced changes to intracellular biomolecules in live leukemia cells. Vib. Spectrosc. 53, 39–44. doi:10.1016/j.vibspec.2010.02.004

Notingher, I., Verrier, S., Haque, S., Polak, J., Hench, L., 2003. Spectroscopic study of human lung epithelial cells (A549) in culture: living cells versus dead cells. Biopolymers 72, 230–240.

Rich, A., Zhang, S., 2003. Z-DNA: the long road to biological function. Nat. Rev. Genet. 4, 566–573.

Stander, A., Marais, S., Stivaktas, V., Vorster, C., Albrecht, C., Lottering, M., Joubert, A.M., 2009. In vitro effects of Sutherlandia frutescens water extracts on cell numbers , morphology , cell cycle progression and cell death in a tumorigenic and a non-tumorigenic epithelial breast cell line. J. Ethnopharmacol. 124, 45–60. doi:10.1016/j.jep.2009.04.013

Summers, K.C., Shen, F., Sierra Potchanant, E.A., Phipps, E.A., Hickey, R.J., Malkas, L.H., 2011. Phosphorylation: the molecular switch of double-strand break repair. Int. J. Proteomics 373816–373824. doi:10.1155/2011/373816

Tinari, A., Giammarioli, A.M., Manganelli, V., Ciarlo, L., Malorni, W., 2008. Analyzing Morphological and Ultrastructural Features in Cell Death. Methods in emzymology 442, 1–26. doi:10.1016/S0076-6879(08)01401-8

Van der Merwe, C.F., Coetzee, J., 1992. Quetol 651 for general use: a revised formulation. Commun. Electron Microsc. Soc. South. Africa 22, 31–32.

Venter, E., Van Der Merwe, C.F., Buys, A. V, Huismans, H., Van Staden, V., 2014. Comparative ultrastructural characterization of African horse sickness virus-infected mammalian and insect cells reveals a novel potential virus release mechanism from insect cells. J. Gen. Virol. 95, 642–651. doi:10.1099/vir.0.060400-0

Vermes, I., Haanen, C., Reutelingsperger, C., 2000. Flow cytometry of apoptotic cell death. J. Immunol. Methods 243, 167–190.

Waggoner, S.E., 2003. Cervical cancer. Lancet 361, 2217–2225.

Yadav, N., Pliss, a, Kuzmin, a, Rapali, P., Sun, L., Prasad, P., Chandra, D., 2014. Transformations of the macromolecular landscape at mitochondria during DNA-damage-induced apoptotic cell death. Cell Death Dis. 5, e1453. doi:10.1038/cddis.2014.405

Zelig, U., Kapelushnik, J., Moreh, R., Mordechai, S., Nathan, I., 2009. Diagnosis of Cell Death by Means of Infrared Spectroscopy. Biophys. J. 97, 2107–2114. doi:10.1016/j.bpj.2009.07.026